Dynamics of concentric and eccentric compound droplets suspended in extensional flows

Xiaofeng Qu and Yechun Wang

Citation: Phys. Fluids **24**, 123302 (2012); doi: 10.1063/1.4770294
View online: http://dx.doi.org/10.1063/1.4770294
View Table of Contents: http://pof.aip.org/resource/1/PHFLE6/v24/i12
Published by the American Institute of Physics.

PHYSICS OF FLUIDS **24**, 123302 (2012)

Dynamics of concentric and eccentric compound droplets suspended in extensional flows

Xiaofeng Qu and Yechun Wang[a)]
Department of Mechanical Engineering, North Dakota State University, Dept. 2490, P.O. Box 6050, Fargo, North Dakota 58108, USA

(Received 18 February 2012; accepted 6 November 2012; published online 11 December 2012)

The motion, deformation, and stability of compound droplets in extensional flows are investigated numerically via a three-dimensional spectral boundary element method. We examine the droplet stability under the influences of the capillary number, the inner droplet size and the relative magnitude of the surface tension of the two interfaces composing the compound droplet. The influence of viscosity on the droplet deformation is also discussed. We conclude that a compound droplet with a larger inner droplet and/or smaller inner surface tension is less stable and cannot withstand strong flow. For moderate viscosity ratios, a compound droplet with a more viscous "shell" exhibits larger deformation at steady state. In addition, for an eccentric compound droplet, both the inner and outer droplets tend to migrate away from its original location due to the asymmetry of the problem. The initial location of the inner droplet also influences the droplet stability as well as the migration velocity of the compound droplet. © *2012 American Institute of Physics*. [http://dx.doi.org/10.1063/1.4770294]

I. INTRODUCTION

Compound droplets are fluid particles consisted of an inner droplet (Fluid 1) encapsulated by another immiscible fluid (Fluid 2) which is itself suspended in a third fluid (Fluid 3) as illustrated in Fig. 1. The term "compound droplets" is used interchangeably with "double emulsions," "globules," or "encapsulated droplets" in the literature. Great interest in the dynamics of viscous compound droplets has been raised due to the applications in drug delivery,[1] materials processing,[2] waste water treatment,[3] food processing,[4] cosmetic applications[5] tissue epitaxy,[6,7] and modeling of blood cells.[8–12] In addition, compound droplets have been observed to exist in the late stages of phase separations[13] as well as in the porous structures of oil reservoirs during enhanced oil recovery.[14] In spite of the growing demand of theoretical investigation of the behavior of compound droplets from the aforementioned applications, very limited effort has been contributed in analytical and/or numerical study of compound droplets.

Since the theoretical analysis of the behavior of rigid compound droplets in quiescent flow by Torza and Mason in 1970,[15] the deformation, relaxation, and stability of viscous compound droplets freely suspended in linear flows have been investigated both analytically and computationally. Torza and Mason[15] categorized compound droplets into three types based on their static configurations: complete engulfing, partial engulfing, and non-engulfing compound droplets. A complete engulfing droplet consists of a smaller droplet completely enclosed by a larger droplet without having the two interfaces touching each other. A partial engulfing compound droplet could be defined by the existence of a three-phase contact line, and may spontaneously form during emulsification and appear like "two drops stuck together." Non-engulfing droplets are referred to as a pair of simple droplets. Fluids in both droplets are enclosed by the same suspending fluid. The static compound droplet configurations are determined by interfacial tension ratios and relative volumes of fluids.[15,16] This study is focused on complete engulfing droplets as described in Fig. 1 under the influence

a)yechun.wang@ndsu.edu.

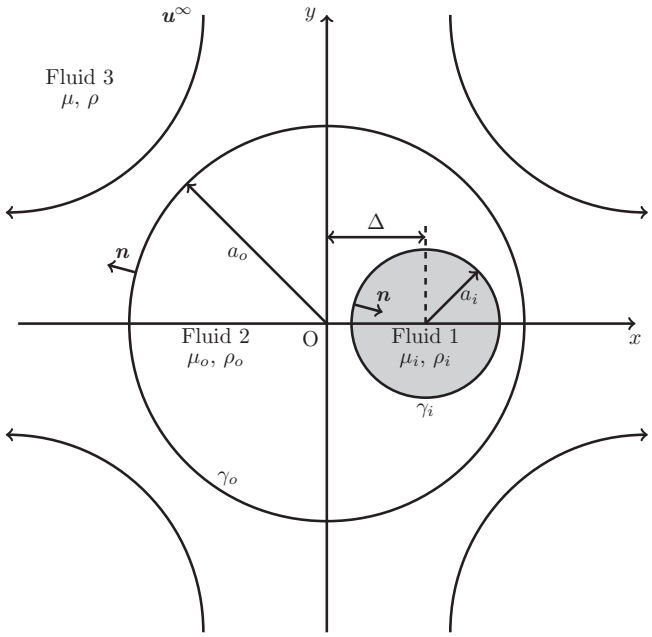

FIG. 1. Schematic of a compound droplet freely suspended in a planar extensional flow with undisturbed velocity $\boldsymbol{u}^\infty = G(x, -y, 0)$.

of extensional flows. The fluid motion and the resulted viscous forces may create dynamically stable complete engulfing droplets for interfacial tension ranges that may lead to different static configurations. If, during the computation of the transient configuration of the compound droplet, the inner and outer interfaces of an initially complete engulfing droplet touch each other, we consider that the complete engulfing compound droplet no longer exists, or, for simplicity, no stable compound droplet exists.

By perturbation analysis, Davis and Brenner[17] investigated the stability of spherical compound droplets with the inner "droplet" as a solid particle which is concentrically placed in the outer droplet (concentric compound droplet). Using the lubrication theory, Sadhal and Johnson[18] analytically predicted the translation of undeformable liquid droplets and gas bubbles coated with a thin layer of surfactant. Rushton and Davies[19] also theoretically derived the drag coefficient and terminal settling velocity of spherical compound droplets rising in a third immiscible fluid. Sadhal and Oguz[20] studied analytically the translation of an eccentric compound droplet in a uniform flow. Undeformed spherical droplets were assumed in their study. Stone and Leal[21] investigated analytically via the small-deformation theory the breakup of a concentric compound droplet in linear flow. They also studied larger deformation of the compound droplet numerically using a boundary integral method with axisymmetric assumption. An Eulerian-Lagrangian algorithm for interface tracking has been employed by Kan *et al.*[8] to compute the deformation of a concentric compound droplet subjected to a uniaxial extensional flow and its subsequent recovery when the flow is turned off. While the main focus of that work was the droplet behavior during the recovery, influence of the viscosity of the inner droplet is briefly studied for the compound droplet in a uniaxial flow. However, the inner droplet size was fixed since the parameters chosen in that work are based on experiments using leukocytes in which the nucleus occupies a volume of 21% of the entire cell. Using a level-set method, Smith *et al.*[22] investigated the behavior of a viscous compound droplet in shear flow and during the recovery. In that study, the viscosities of all phases are equal and the inner droplet size is half of that of the outer droplet. Smith *et al.*[22] focused on the investigation of the influence of the relative magnitude of the surface tensions of the two interfaces and provided a phase diagram for the droplet morphology for a variety of capillary number and surface tensions.

In this study, a boundary integral equation is derived for a viscous compound droplet freely suspended in an extensional flow. A fully three-dimensional (3D) spectral boundary element method

has been employed. The algorithm development and validation will provide foundation for future investigations on compound droplet motion in confined flows. In this work, we explore the influences of parameters, including the relative size and surface tension of the two interfaces, the viscosity ratios, capillary number of the outer droplet, and the initial location of the inner droplet in the compound droplet, on the deformation, stability and/or the migration of the compound droplet. We emphasize that besides concentric droplets this work considers the dynamics of initially eccentric compound droplets in planar extensional flows, which was not examined before. In addition, this work investigates the droplet behavior for a wide range of viscosities and surface tension ratios, reveals the configuration of compound droplets in the presence of dynamic forces, and provides in-depth information on the stability of compound droplets in the planar extensional flow.

II. MATHEMATICAL FORMULATION AND NUMERICAL METHOD

As illustrated in Fig. 1, we consider a compound droplet with an inner phase (Fluid 1) with viscosity μ_i and an outer phase (Fluid 2) with viscosity μ_o, freely suspended in a third phase (Fluid 3) with viscosity μ. Due to the small size of the droplet (in micrometers) and our assumption of dominating surface tension force, the Bond number of the current problem is small, $B_{d,o} \to 0$ and $B_{d,i} \to 0$, where $B_{d,o} = (\rho - \rho_o)ga_o^2/\gamma_o$ and $B_{d,i} = (\rho_o - \rho_i)ga_i^2/\gamma_i$. Hence, the influence of the gravity is negligible. Subscripts, "o" and "i," indicate the properties of the outer and inner phases, respectively. All fluids are incompressible, Newtonian and immiscible with each other. The undeformed radius of the outer and inner spherical droplets are a_o and a_i, respectively. We define the droplet size ratio as $k = a_i/a_o$. The surface tension on the interface between Fluids 1 and 2 is γ_i; that between Fluids 2 and 3 is γ_o. We define the surface tension ratio as $\Gamma = \gamma_i/\gamma_o$. By denoting the viscosity of Fluid 3 as μ, the viscosities of the outer phase (Fluid 2) and inner phase (Fluid 1) are designated as $\mu_o = \lambda_o\mu$ and $\mu_i = \lambda_i\mu$, respectively. In addition, the distance between the centroids of the outer and inner droplets is denoted as $\Delta = \delta a_o$. We investigate the deformation of a compound droplet in extensional flows, e.g., a planar extensional flow, $\boldsymbol{u}^\infty = G(x, -y, 0)$, where G is the shear rate. The deformation of a droplet is quantified by $D = (l_1 - l_2)/(l_1 + l_2)$, where l_1 is the longest axis of the droplet and l_2 is the shortest axis. D_o and D_i designate the deformations of the outer and inner interfaces of a compound droplet, respectively. In this work, we employ the radius of the initially spherical outer droplet a_o as the length scale, Ga_o as the velocity scale, and thus $1/G$ the time scale. As the measure of the relative importance of viscous force and surface tension, the capillary numbers for the outer and inner droplets are defined, respectively, by

$$Ca_o = \frac{\mu G a_o}{\gamma_o}, \tag{1}$$

$$Ca_i = \frac{\mu_o G a_i}{\gamma_i} = \frac{\lambda_o k}{\Gamma} Ca_o. \tag{2}$$

Under low-Reynolds-number assumptions, the governing equations are the Stokes equation and the continuity,

$$\nabla \cdot \boldsymbol{\sigma} = -\nabla p + c\nabla^2 \boldsymbol{u} = \boldsymbol{0}, \tag{3}$$

$$\nabla \cdot \boldsymbol{u} = 0, \tag{4}$$

where $c = \mu_i$, μ_o, and μ for Fluids 1–3, respectively. The pressure as defined in Eq. (3) is the dynamic pressure.

The boundary conditions for the velocity $\boldsymbol{u}$ and force $\boldsymbol{f}$ on the inner interface of the compound droplet are

$$\boldsymbol{u}_1 = \boldsymbol{u}_2, \tag{5}$$

$$\Delta \boldsymbol{f} = \boldsymbol{f}_1 - \boldsymbol{f}_2 = \frac{\Gamma}{Ca_o}(\nabla_S \cdot \boldsymbol{n})\boldsymbol{n}, \tag{6}$$

while the boundary conditions on the outer interface give

$$\boldsymbol{u}_2 = \boldsymbol{u}_3, \tag{7}$$

$$\Delta \boldsymbol{f} = \boldsymbol{f}_3 - \boldsymbol{f}_2 = \frac{1}{Ca_o}(\nabla_S \cdot \boldsymbol{n})\boldsymbol{n}. \tag{8}$$

The subscripts designate quantities evaluated in Fluids 1–3, respectively. The surface stress is defined as $\boldsymbol{f} = \boldsymbol{\sigma} \cdot \boldsymbol{n}$, where the unit normal $\boldsymbol{n}$ is defined to point into Fluids 1 and 3 for the inner and outer interfaces, respectively.

The following boundary integral equation could be derived[23] and employed to determine the velocity at any geometric point on the interface of the compound droplet

$$\begin{aligned}\Omega \boldsymbol{u} - \Omega_o \boldsymbol{u}^\infty = &- \frac{1}{4\pi\mu}\int_{S_o} [\boldsymbol{S}\cdot\Delta\boldsymbol{f} - (1-\lambda_o)\,\mu\,\boldsymbol{T}\cdot\boldsymbol{u}\cdot\boldsymbol{n}]dS \\ &- \frac{1}{4\pi\mu}\int_{S_i} [\boldsymbol{S}\cdot\Delta\boldsymbol{f} - (\lambda_i-\lambda_o)\,\mu\,\boldsymbol{T}\cdot\boldsymbol{u}\cdot\boldsymbol{n}]dS,\end{aligned} \tag{9}$$

where $\Omega = 1 + \lambda_o$ and $\Omega_o = 2$ for the outer interface S_o and $\Omega = \lambda_i + \lambda_o$ and $\Omega_o = 2\lambda_i$ for the inner interface S_i. Kernel $\boldsymbol{S}$ is the fundamental solution for the three-dimensional Stokes equations and $\boldsymbol{T}$ is the associated stress defined by

$$S_{ij} = \frac{\delta_{ij}}{r} + \frac{\hat{x}_i\hat{x}_j}{r^3},\ T_{ijk} = -6\frac{\hat{x}_i\hat{x}_j\hat{x}_k}{r^5}, \tag{10}$$

where $\hat{\boldsymbol{x}} = \boldsymbol{x} - \boldsymbol{x}_0$ and $r = |\hat{\boldsymbol{x}}|$.[23]

Both the inner and outer interfaces of the compound droplet are discretized into $N_E = 6$ quadrilateral spectral elements as shown in Fig. 2 via cube projection. The geometric variables on each element can be obtained by Lagrange interpolations using two parametric variables on a square interval $[-1, 1]^2$. The basis points for the parametric variables are zeros of N_B-order orthogonal polynomials and hence they are spectral points. Therefore, we have a total number of $N = 2\,N_E\,N_B^2$ spectral points for the compound droplet. The geometric and physical information on discretized node is then substituted into the boundary integral equation (Eq. (9)). By rearrangement and collection of terms, a linear system of algebraic equations relating the velocity $\boldsymbol{u}$ and stress $\boldsymbol{f}$ is formed $\boldsymbol{u} = \boldsymbol{A}\boldsymbol{f} + \boldsymbol{B}\boldsymbol{u}$. The matrices A and B are obtained by the integration of the kernels $\boldsymbol{S}$ and $\boldsymbol{T}$. Gauss quadrature with Legendre and Lobatto points are employed for the integrations. Gauss elimination is then used to solve the linear system for the velocity. With the values of velocity for all geometric points ($\boldsymbol{x}$) on the interface, a fourth-order Runge-Kutta algorithm is employed to find the time evolution of the interface geometry using the following kinematic condition:

$$\frac{d\boldsymbol{x}}{dt} = (\boldsymbol{u}\cdot\boldsymbol{n})\boldsymbol{n}. \tag{11}$$

In addition, interfacial smooth schemes and mesh redistribution techniques have been employed. The details can be found in Wang and Dimitrakopoulos.[24] Similar techniques have also been employed in Refs. 25 and 26. In this work, we employ $N_B = 11$ spectral points in one curvilinear direction for each element. This is based on our convergence tests as shown in Fig. 3, which plots the relative error in droplet deformation D_o and D_i as a function of the total number of spectral points used $N = 2N_EN_B^2$. Basis points $N_B = 5, 7, 9, 11, 13$ are employed in the computation. Results for $N_B = 15$ are used as the base in computing the relative error. An exponential convergence in numerical accuracy in computing the droplet deformation is observed. Using $N_B = 11$ spectral points gives an accuracy in the order of magnitude of 10^{-5}.

We emphasize that our numerical approach, a three-dimensional spectral boundary element method for interfacial dynamics in Stokes flow, is able to capture the dynamics of compound droplets efficiently by computing only for the interfacial evolution without the need to obtain flow information in the fluid volume. By using a high-order algorithm with spectral discretization on the droplet interface, the method exploits all the benefits of spectral methods, i.e., exponential

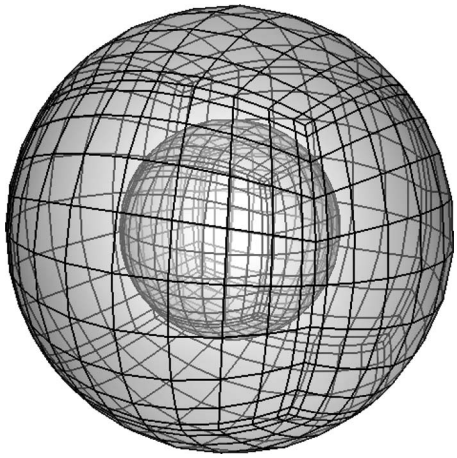

FIG. 2. Discretization of a compound droplet with spectral elements.

convergence and numerical stability, with the versatility of the finite element method, i.e., the ability to handle complicated geometries.[24]

III. RESULTS AND DISCUSSION

Using the 3D spectral boundary element method with the newly derived integral equation for compound droplets, we computationally investigate the deformation and stability of compound droplets in a planar extensional flow. As shown in Fig 4(a), the deformation of the outer droplet D_o increases with the outer capillary number Ca_o. This behavior is similar to that of a single droplet although the magnitude of the deformation may differ. We also obtain the deformation of the inner droplet D_i as a function of the non-dimensionalized time t and the outer capillary number Ca_o, which is shown in Fig. 4(b). We observe that steady-state deformation of the inner droplet also monotonically increases with Ca_o, while the magnitude of the deformation is smaller than that of the outer droplet D_o.

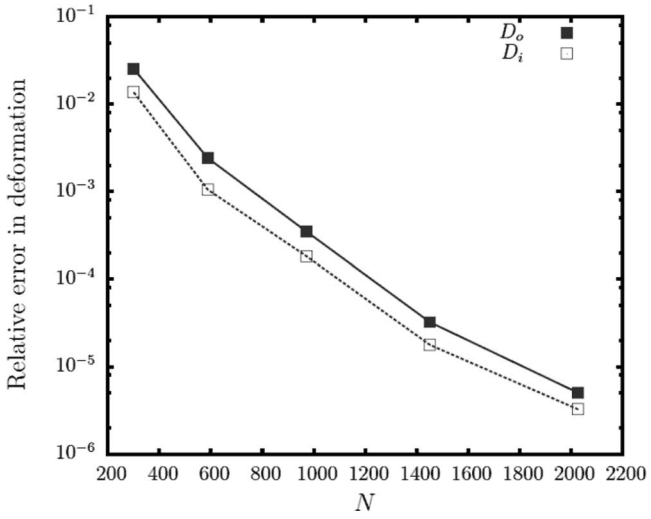

FIG. 3. The relative error in computed steady-state deformation D_i and D_o versus the number of spectral points $N = 2N_E N_B^2$ for a concentric compound droplet with $Ca_o = 0.06$, $k = 0.1$, $\Gamma = 1$, and $\lambda_o = \lambda_i = 1$ suspended in a uniaxial extensional flow. $N_E = 6$ spectral elements are used for each interface in the compound droplet. Results for basis points $N_B = 5, 7, 9, 11, 13$ are shown with that for $N_B = 15$ as the base in computing the relative error.

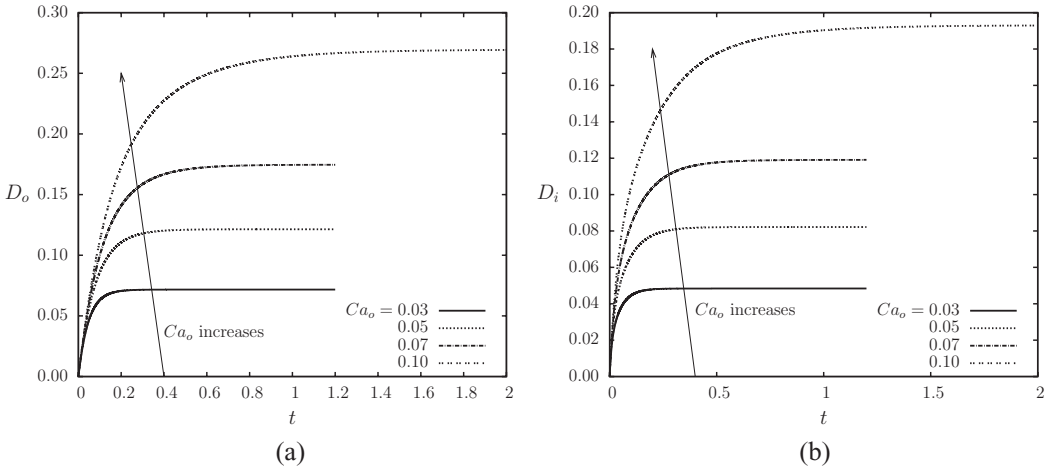

FIG. 4. Deformation of the (a) outer and (b) inner droplets as a function of time t and capillary number Ca_o in a two-dimensional extensional flow. For all cases, $k = 0.4$, $\Gamma = 0.7$, and $\lambda_o = \lambda_i = 0.2$.

In this section, we first compare our numerical results in droplet deformation with analytical predictions and other numerical findings. We then present the influence of the relative size of the inner droplet, surface tension ratio as well as viscosity ratio on the behavior of the compound droplet. We also illustrate the influence of an inner droplet eccentrically located in the outer droplet on the behavior of the entire compound droplet.

A. Validation

To validate our numerical approach, we compare our results by 3D spectral boundary element method with the analytical predictions and numerical results with axisymmetric assumption by Stone and Leal.[21] Figure 5 shows the deformation of a compound droplet in a uniaxial flow, $\boldsymbol{u}^\infty = G(-x/2, -y/2, 2z)$, for $\lambda_o = \lambda_i = 1.0$, $\Gamma = 1.0$, and $k = 0.5$. Results using our 3D spectral boundary element method and the aforementioned study are included. We observe that for small

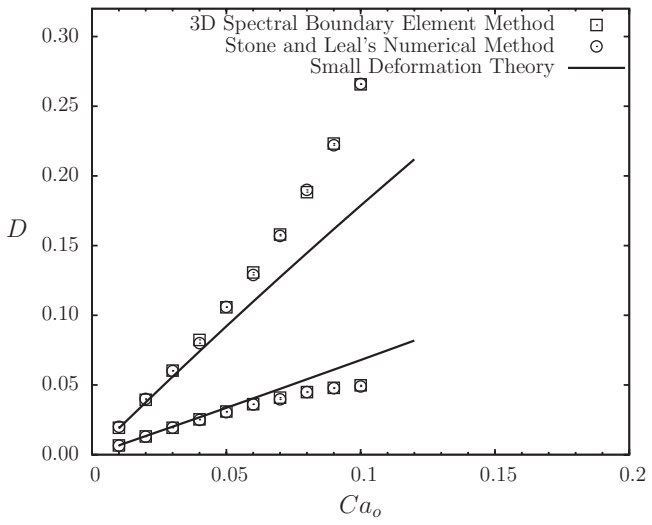

FIG. 5. Steady-state deformation for the outer (upper curves) and inner (lower curves) droplets of a compound droplet as a function of the outer capillary number Ca_o. Our computational results (squares) are compared with axisymmetric numerical results (circles) and analytical predictions (solid lines) by Stone and Leal[21] for a compound droplet suspended in a uniaxial flow for $\lambda_o = \lambda_i = 1.0$, $\Gamma = 1.0$, and $k = 0.5$.

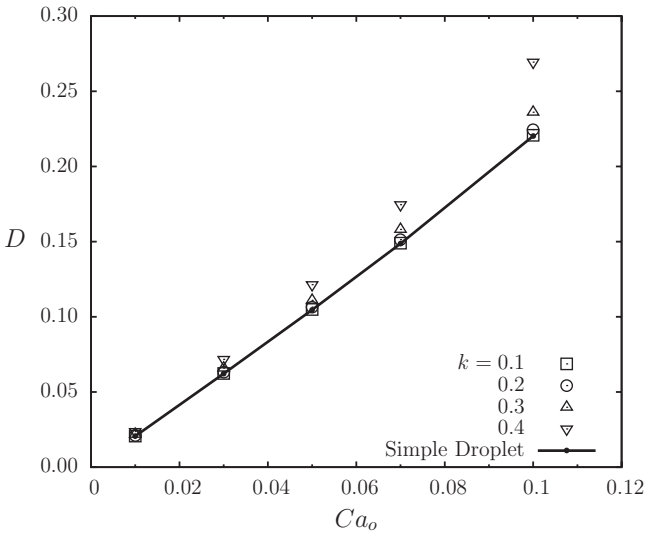

FIG. 6. Steady-state droplet deformation as a function of the (outer) capillary number for the outer interface of a compound droplet (triangles, circles, and squares) and a simple droplet (dots) suspended in a planar extensional flow. For the compound droplet, $\Gamma = 0.7$ and $\lambda_o = \lambda_i = 0.2$. A variety of values for k has been included. For the simple droplet, the viscosity ratio between the droplet and the suspending fluid is 0.2.

values of the capillary number Ca_o, our numerical results agree well with both analytical and numerical results of previous work, while for larger Ca_o, agreement is only found among numerical results since the analytical method assumes nearly spherical droplets.

If the inner droplet size is infinitely small, the deformation of the outer droplet of a compound droplet should behave similar to a simple droplet (i.e., a single droplet without the inner droplet). This should be revealed by computation if the algorithm is correct. As shown in Fig. 6, we plot the steady-state deformation of the outer interface of a compound droplet as a function of the outer capillary number. Several values for the size ratio (k) have been included. In the same figure, we also plot the deformation of a simple droplet with the same flow conditions for comparison. We observe that the deformation D for the outer interface of a compound droplet approaches that of a simple droplet as k decreases. When the size of the inner droplet is one tenth of that of the outer droplet, $k = 0.1$, excellent agreement is found between outer interface deformation and simple droplet deformation. The transient behavior of the deformation for a droplet with or without a small inner droplet ($k = 0.1$) is also found to be similar.

B. Influence of the size ratio

To examine the influence of the existence or the size of an inner droplet on the deformation and stability of a compound droplet, we plot the time evolution of the deformation of the outer droplet D_o in Fig. 7(a). We find the increase of the inner droplet size k results in significant increase of the deformation of the outer droplet. This is in agreement with findings by Davis and Brenner[17] for compound droplets with a solid inner phase and by Stone and Leal[21] for fluid inner phase. When the inner droplet size exceeds a critical value, the outer droplet deformation increases extensively and no steady-state shapes could be found. This finding implies that the flow conditions which retain stable single droplets may lead to unstable compound droplets if a moderate sized inner droplet resides in the outer droplet and that the size of the inner droplet also determines the droplet stability. As it is influencing the outer droplet deformation, the deformation of the inner droplet itself is also affected by its size relative to that of the outer droplet. As shown in Fig. 7(b), as k increases, the inner droplet deformation D_i also increases, and no steady state could be found after k exceeds a critical value. In the particular example shown in Fig. 7, the critical size ratio is found to be $k_c = 0.59$.

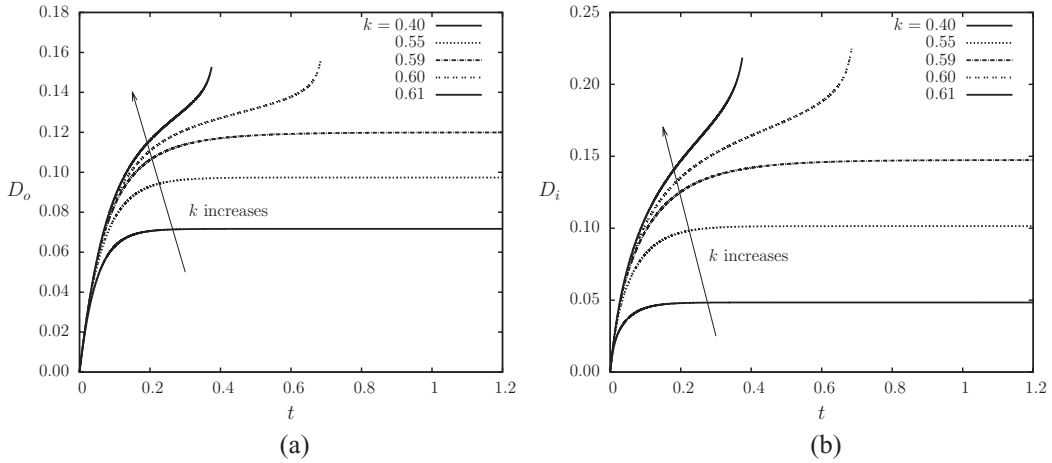

FIG. 7. Deformation of the (a) outer and (b) inner droplets as a function of time t and size ratio k. For all cases, $Ca_o = 0.03$, $\Gamma = 0.7$, and $\lambda_o = \lambda_i = 0.2$.

We believe that the instability of the compound droplet may lie in the formation and snap-off of the thin film between the outer and inner droplets. Figure 8 shows an example in which the minimum distance d_{min} between the inner and outer interfaces decreases at the early stage of droplet deformation. For a compound droplet with a relatively smaller inner droplet (i.e., smaller values for k), the minimum distance d_{min} may reach a constant value at the steady state. As k increases, the steady-state d_{min} decreases. However, for a compound droplet with a larger inner droplet, the minimum distance decreases abruptly at the moment when the inner and outer interfaces approach close to each other with a thin film formed between them ($d_{min} \to 0$). This may lead to the break up of the droplet or the formation of a partially engulfing compound droplet which is out of the scope of the current study. We plot the time evolution of droplet profiles in Fig. 9 for a situation in which no steady state exists for the compound droplet. We observe that the initially spherical outer droplet deforms into an prolate spheroidal shape due to the external planar extensional flow imposed. The fluid inside the outer droplet is also been driven to flow in the form of an extensional-like flow, hence the inner droplet also elongates into a prolate spheroidal shape with its long axis perpendicular

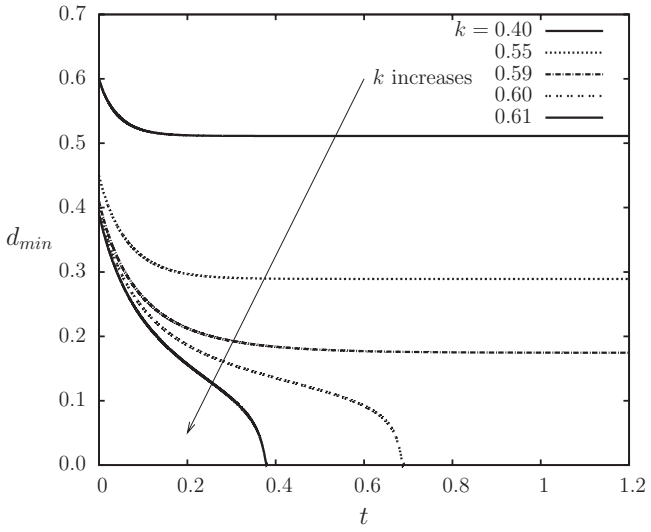

FIG. 8. The minimum distance d_{min} between the outer and inner droplets as a function of time t for a compound droplet suspended in a 2D extensional flow. For all cases, $Ca_o = 0.03$, $\Gamma = 0.7$, and $\lambda_o = \lambda_i = 0.2$.

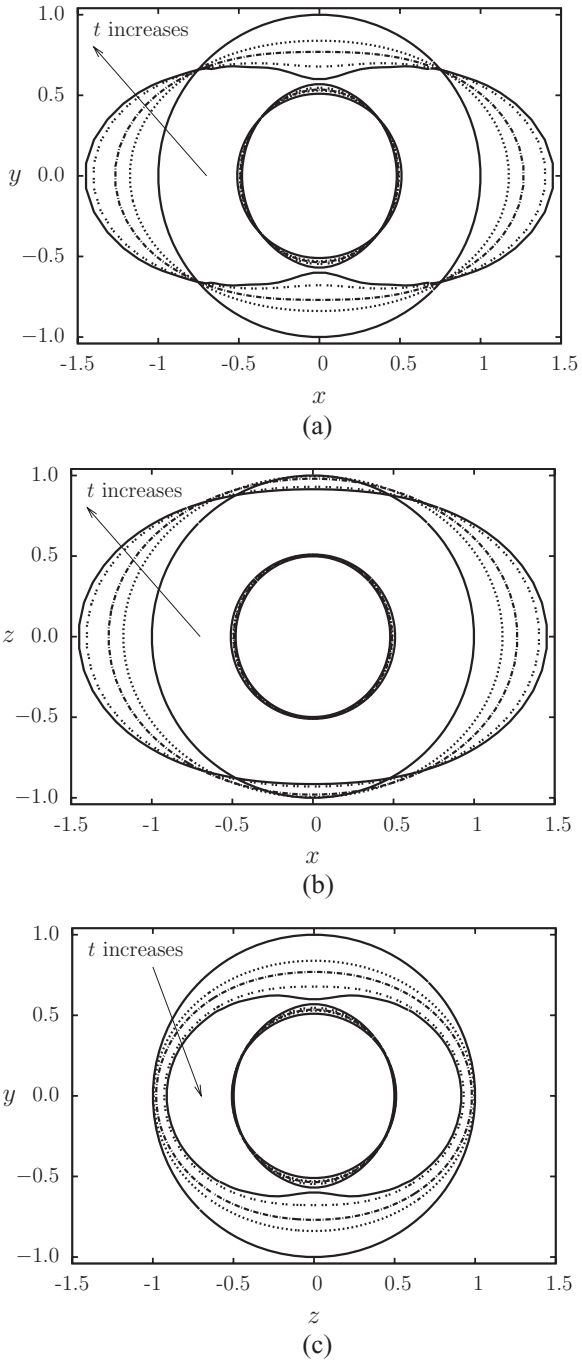

FIG. 9. Time evolution of droplet profiles at *xy*, *xz*, and *zy* planes for a compound droplet deforming in a planar extensional flow. (a)–(c) $Ca_o = 0.1$, $k = 0.51$, $\Gamma = 4$, and $\lambda_o = \lambda_i = 0.2$. Profiles are plotted for time $t = 0$, 0.15, 0.3, 0.9, 1.44.

to that of the outer droplet. As the two interfaces approach each other, dimples and sharp ends are developed on the outer and inner interfaces, respectively. The three-dimensional shapes right before the close contact of the two interfaces are plotted in Fig. 10 which shows the dimples developed in the center of the outer droplet and the sharp ends formed on the inner droplet. Besides the contact of the two interfaces, the deformability of the interfaces also contributes in the stability of the compound droplet since the breakup of either the inner or the outer droplet may also lead to

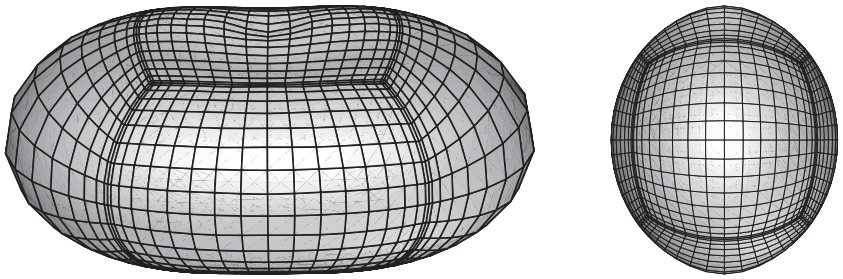

FIG. 10. 3D geometries for the deformed (a) outer and (b) inner droplet at $t = 1.44$. $Ca_o = 0.1$, $k = 0.51$, $\Gamma = 4$, $\lambda_o = \lambda_i = 0.2$.

the instability of the compound droplet. Hence, we investigate in a similar fashion for the stability of a compound droplet with a variety of values for the outer capillary number and plot in Fig. 11 the critical size ratio k_c as a function of Ca_o. As shown in the figure, we are able to find stable compound droplets with large inner droplet when the outer capillary number is small. For situations below the curve, steady-state exists for compound droplets. Curves are included in the figure for three different values of the surface tension ratio Γ. For smaller Γ, i.e., more deformable inner droplet, the critical size ratio k_c becomes smaller.

C. Influence of the surface tension ratio

When the outer capillary number is kept constant, varying the surface tension ratio Γ could be considered as altering the relative deformability of the inner droplet. As shown in Fig. 12(a), the steady-state deformation of the inner droplet D_i increases as we decrease Γ. When Γ becomes less than a critical value Γ_c, no steady-state shape could be found. The deformation of the outer droplet is also affected similarly by the surface tension ratio although the influence is much smaller, as shown in Fig. 12(b). We believe that when the surface tension of the inner droplet is much less than that of the outer droplet (i.e., $\Gamma < \Gamma_c$), the severe deformation/elongation and eventually the breakup of the inner droplet lead to the instability of the entire compound droplet. This can be elucidated by

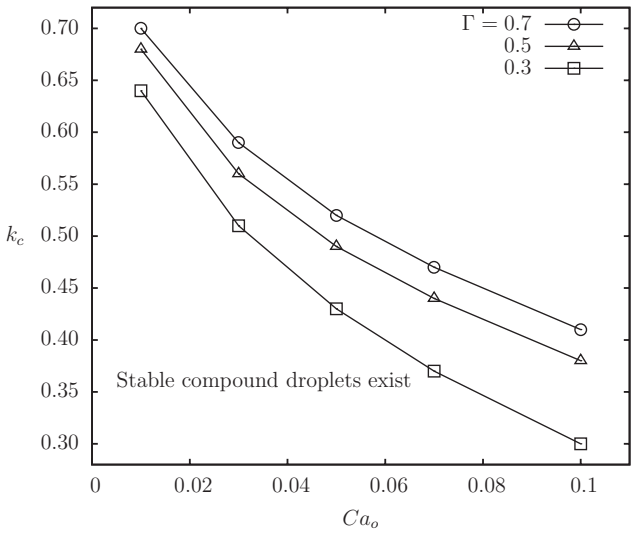

FIG. 11. Critical size ratio k_c as a function of the outer capillary number Ca_o. Three cases are plotted with $\Gamma = 0.3$, 0.5, and 0.7. For all results shown, $\lambda_o = \lambda_i = 0.2$.

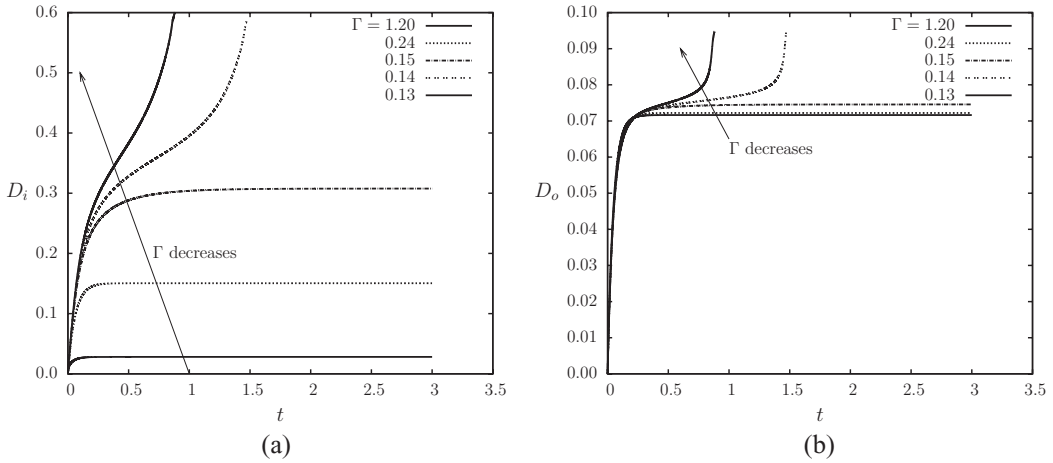

FIG. 12. Deformation of the (a) inner and (b) outer droplets as a function of time t and surface tension ratio Γ in a planar extensional flow. For all cases, $Ca_o = 0.03$, $k = 0.4$, and $\lambda_o = \lambda_i = 0.2$.

plotting the time evolution of the profiles of a compound droplet with a small Γ. Figure 13 shows the profiles of a compound droplet with $Ca_o = 0.03$, $k = 0.4$, $\Gamma = 0.14$, and $\lambda_o = \lambda_i = 0.2$. We observe that the inner droplet deforms much more severely than the outer droplet. The instability or the extensive deformation of the inner droplet leads finally to the breakup of the entire compound droplet.

For the example shown in Fig. 12, the critical surface tension ratio is found to be $\Gamma_c = 0.15$. We have investigated the influence of Γ on the stability of compound droplets for a variety of values of the outer capillary number and plot in Fig. 14 the critical surface tension ratio Γ_c as a function of Ca_o. We notice that as the outer capillary number increases, the critical surface tension ratio Γ_c increases. For situations above the curve, stable compound droplets may be found. We could interpret the results as that the compound droplet can maintain stable in stronger flows if the inner interface is less deformable. Results for three different values of size ratio k are included. For larger k, Γ_c increases more substantially with Ca_o, hence, we understand that for larger inner droplet a much less deformable inner interface is required for the compound droplet to stay stable in stronger flows.

D. Influence of viscosity ratios

We also explore the influence of the relative viscosities of fluids on the deformation of the freely suspended compound droplet. Figure 15 shows the steady-state deformation of the inner and outer droplets, D_i and D_o, as a function of the outer viscosity ratio λ_o, while the inner viscosity ratio is maintained constant, $\lambda_i = 1$. In the range of $10^{-2} \le \lambda_o \le 10$, both the inner and outer droplets show substantial increase with λ_o. This implies that compound droplets with a more viscous "shell" tend to deform more significantly for moderate values of λ_o. For compound droplets with extremely small or large λ_o, e.g., $\lambda_o < 10^{-2}$ or $\lambda_o > 10$, the droplet deformation is found almost independent on λ_o. Figure 16 presents the steady-state deformation, D_i and D_o, as a function of the inner viscosity ratio λ_i, while we keep the outer viscosity ratio constant, $\lambda_o = 1$. We observe that for small values of the inner viscosity ratio, e.g., $\lambda_i < 10^{-2}$, D_i and D_o are independent on the inner viscosity ratio. When $\lambda_i > O(10^{-2})$, the deformation of both the outer and inner droplets decreases significantly as we increase λ_i. Besides examples shown in Figs. 15 and 16, computations with other parameters exhibit similar behavior for a stable compound droplet. We conclude that the deformation of the inner and outer droplets shows great dependency on viscosities for moderate viscosity ratios between $O(10^{-1})$ and $O(1)$. The compound droplet exhibits larger deformation if the outer droplet is more viscous, or the inner droplet is less viscous.

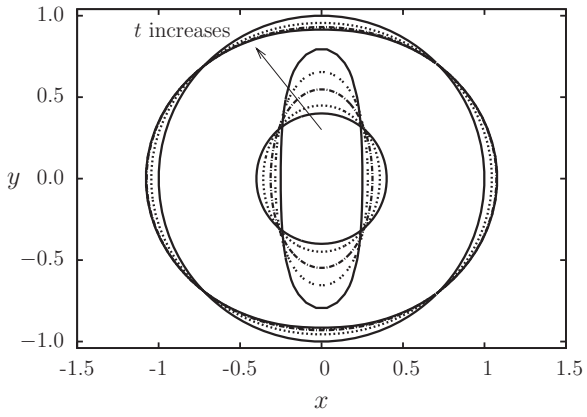

(a)

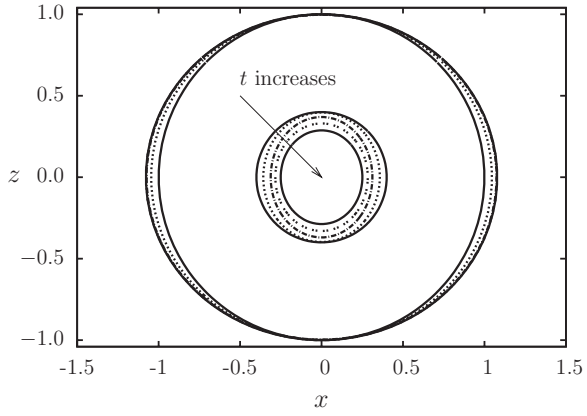

(b)

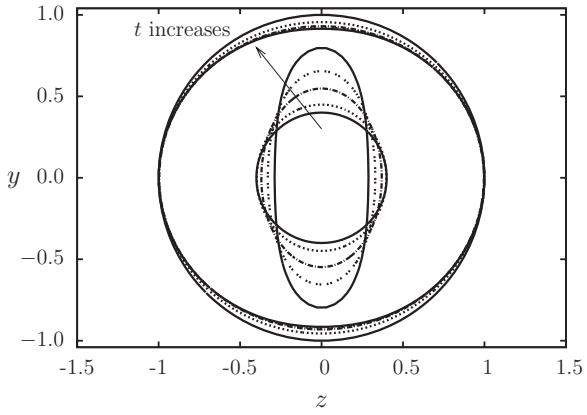

(c)

FIG. 13. Time evolution of droplet profiles at *xy*, *xz*, and *zy* planes for a compound droplet deforming in a planar extensional flow. (a)–(c) $Ca_o = 0.03$, $k = 0.4$, $\Gamma = 0.14$, and $\lambda_o = \lambda_i = 0.2$. Profiles are plotted for time $t = 0$, 0.05, 0.25, 1, 1.4.

E. Eccentric compound droplets

It is of great theoretical interest to investigate the behavior of freely suspended compound droplets with the inner droplet eccentrically located in the outer droplet, i.e., eccentric compound droplets. Benefit from the fully three-dimensional numerical scheme, we compute the transient deformation and migration of an eccentric compound droplet in a planar extensional flow. The

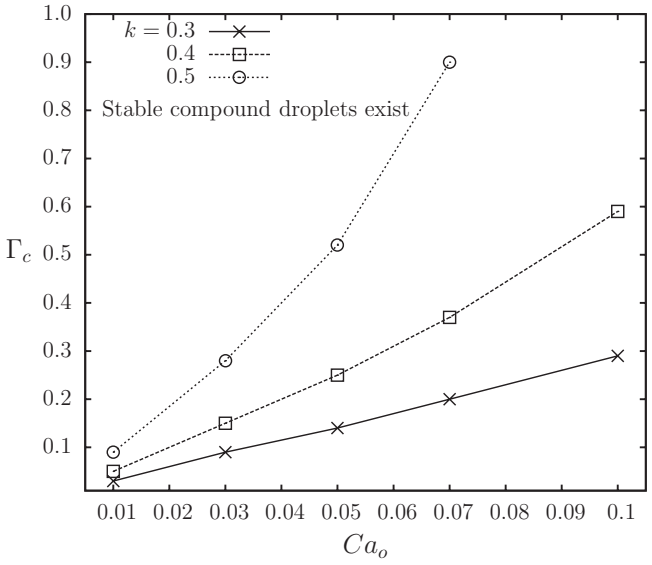

FIG. 14. Critical surface tension ratio Γ_c as a function of the outer capillary number Ca_o. Three cases are plotted with $k = 0.3$, 0.4, and 0.5. For all results shown, $\lambda_o = \lambda_i = 0.2$.

centroid of the outer droplet is initially located at the origin, i.e., (0, 0, 0), of the coordinate system defining the extensional flow, while the inner droplet is initially positioned on the x axis, y axis, or $y = x$ with a distance of δ from the origin. The schematic is shown in Fig. 1. The initial shapes of the inner and outer droplets are both spherical.

For an eccentric compound droplet with its inner droplet initially located at (δ, 0, 0), we present two cases among what we explored: (i) an eccentric droplet with all parameters identical to those of a stable concentric droplet and (ii) a droplet with parameters identical to those of an unstable concentric droplet. Figures 17(a) and 17(b) show the behavior of the inner droplet deformation D_i as a function of time t and δ for cases (i) and (ii), respectively. For case (i), we observe that δ modifies slightly the behavior of D_i in the early stage of droplet motion for both cases, while the steady-state

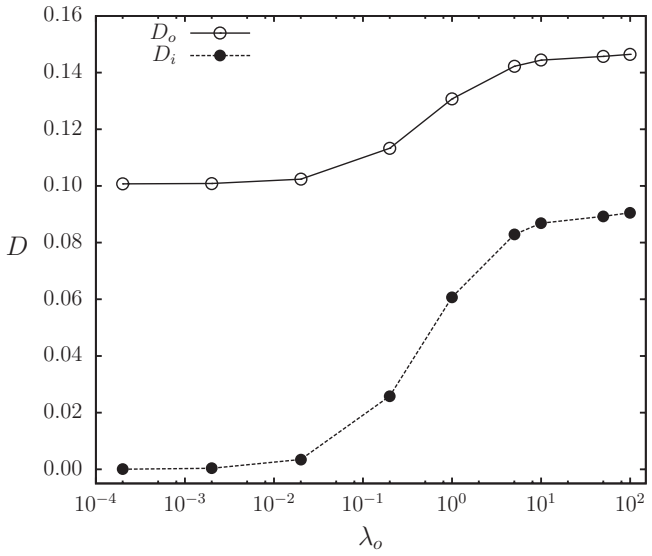

FIG. 15. Steady-state droplet deformation as a function of viscosity ratio λ_o. For all cases, $Ca_o = 0.05$, $k = 0.5$, $\Gamma = 0.7$, and λ_i=1.

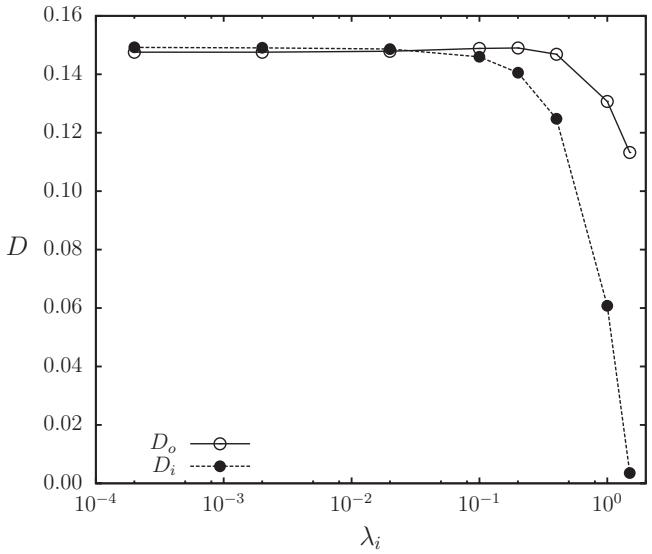

FIG. 16. Steady-state droplet deformation as a function of viscosity ratio λ_i. For all cases, $Ca_o = 0.05$, $k = 0.5$, $\Gamma = 0.7$, and λ_o=1.

deformation of the inner droplet is independent on δ. The influence of δ on D_i is found to be minimal for case (ii). The outer droplet deformation D_o for both cases is found to be independent on δ as shown in Fig. 18.

We plot the time evolution of droplet profiles in the xy plane in Fig. 19. The inner droplet is found to move towards the origin for both cases. Case (ii) shows substantial deformation for both the outer and inner droplets as the inner droplet moves. To quantify the inner droplet motion, we compute the location of the centroid of the inner droplet x_i^c as a function of time, as shown in Fig. 20. For both cases, the inner droplet is eventually trapped at the origin after its initial migration. We also plot the inner droplet velocity $u_{x,i}^c$ as a function of the droplet location x_i^c in Fig. 21. We observe that the inner droplet velocity decreases as the droplet-origin distance δ decreases except for the initial onset of the migration. For a larger value of δ, the droplet migrates with a higher velocity. By plotting the centroid location of the outer droplet x_o^c as a function of time, we observe in Fig. 22 that the outer droplet also moves slightly in the same direction with the inner droplet. The outer droplet travels more distance if the inner droplet is initially located further away from the

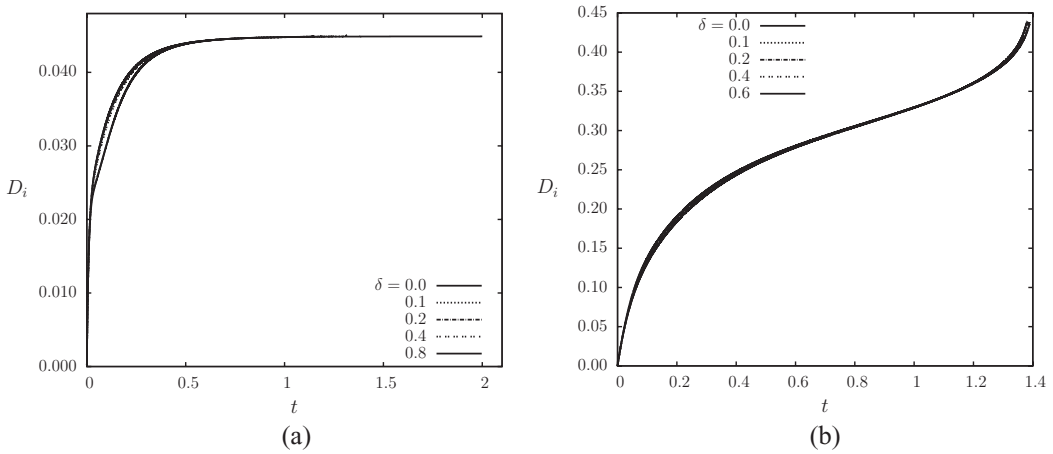

FIG. 17. Inner droplet deformation D_i as a function of time t for a compound droplet with the inner droplet initially located on the x axis. The size ratios are (a) $k = 0.1$ and (b) $k = 0.39$. For all cases, $Ca_o = 0.1$, $\Gamma = 0.5$, and $\lambda_o = \lambda_i = 0.2$.

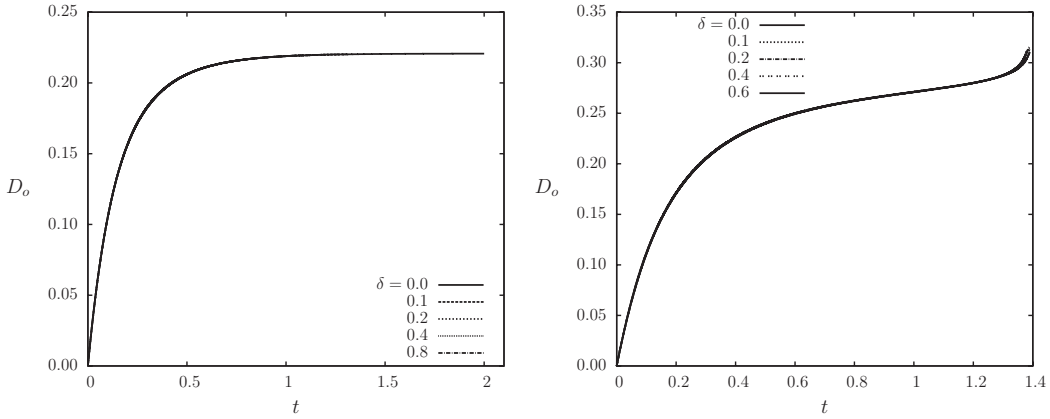

FIG. 18. Outer droplet deformation D_o as a function of time t for a compound droplet with the inner droplet initially located on the x axis. The size ratios are (a) $k = 0.1$ and (b) $k = 0.39$. For all cases, $Ca_o = 0.1$, $\Gamma = 0.5$, and $\lambda_o = \lambda_i = 0.2$.

origin. However, the outer droplet migration is almost indiscernible comparing to the inner droplet motion.

For droplets suspended in a planar extensional flow, no steady state could be found if the inner droplet is initially located on the y axis. As shown in Fig. 23, the inner droplet tends to deform and move towards the outer interface and away from the origin. The contact of the two interfaces will not allow the stable existence of a completely engulfing compound droplet although the parameters that we use in the computation would otherwise lead to a stable concentric droplet. The outer droplet loses its symmetry about x axis due to the formation of a dimple at the close vicinity of the inner droplet. As shown in Fig. 24, where the abrupt increase in deformation D_i indicates the close contact of the two interfaces, a larger δ leads to a easier collision of the two interfaces and a less stable situation. Figure 25 plots the centroid velocity of the inner and outer droplets, $u^c_{y,i}$ and $u^c_{y,o}$, as a function of the droplet location, y^c_i and y^c_o, respectively. The inner droplet shows an accelerated motion towards the outer droplet and away from the origin. The outer droplet is found to migrate slightly away from the origin in the same direction with the inner droplet. For a larger value of δ, the outer droplet moves faster although the magnitude of it is much smaller than that of the inner droplet.

If the inner droplet centroid is located away from both the x and y axes, no steady state could be found for the compound droplet. As an example, Fig. 26 shows the droplet profiles on the xy plane

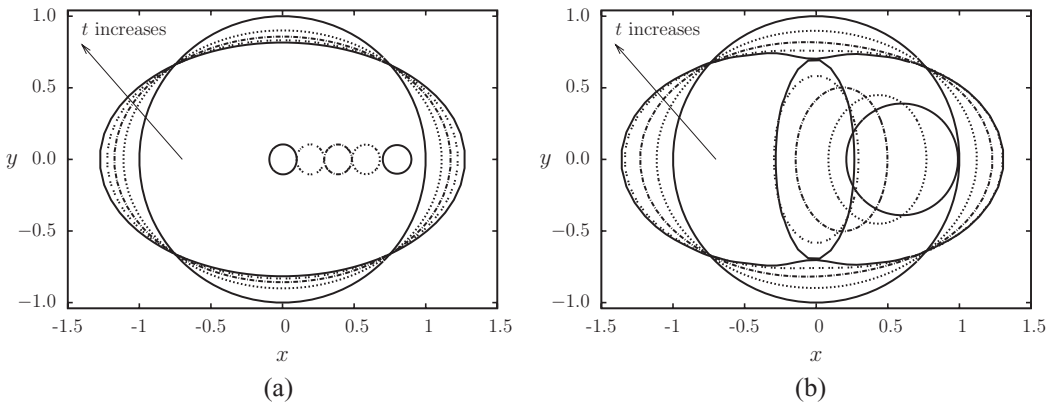

FIG. 19. Profiles of a compound droplet for (a) $Ca_o = 0.1$, $k = 0.1$, $\Gamma = 0.5$, $\lambda_o = \lambda_i = 0.2$, $\delta = 0.8$, $t = 0$, 0.1, 0.2, 0.35, 1.14, and (b) $Ca_o = 0.1$, $k = 0.39$, $\Gamma = 0.5$, $\lambda_o = \lambda_i = 0.2$, $\delta = 0.6$, $t = 0$, 0.1, 0.3, 1, 1.39.

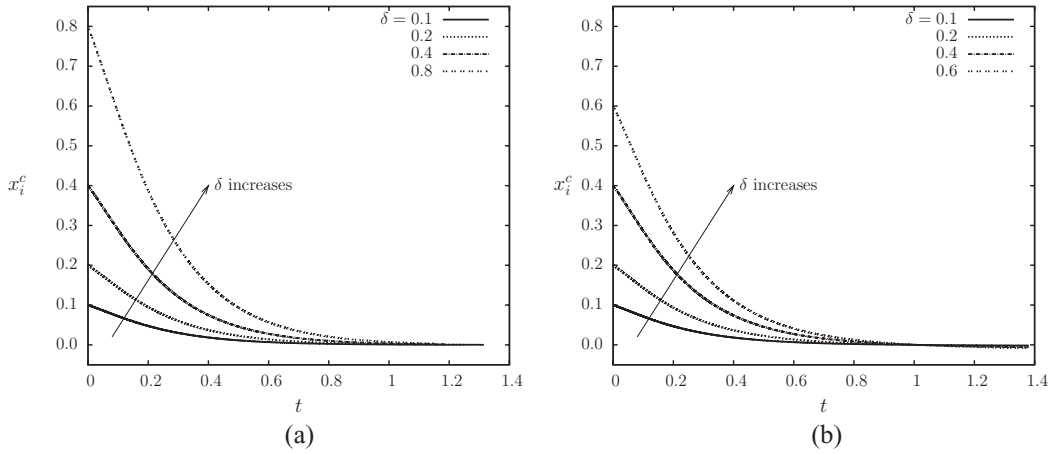

FIG. 20. Droplet location x_i^c of the inner droplet as a function of time t for a compound droplet with the inner droplet located on the x axis. The size ratios are (a) $k = 0.1$ and (b) $k = 0.39$. For all cases, $Ca_o = 0.1$, $\Gamma = 0.5$, $\lambda_o = \lambda_i = 0.2$.

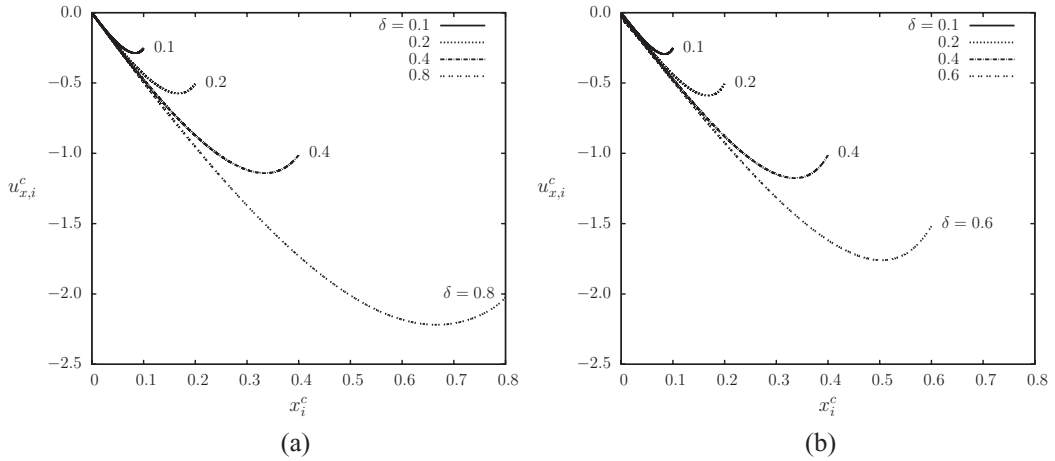

FIG. 21. Velocity of the inner droplet $u_{x,i}^c$ as a function of the droplet location x_i^c. The inner droplet is located on the x axis. The size ratios are (a) $k = 0.1$ and (b) $k = 0.39$. For all cases, $Ca_o = 0.1$, $\Gamma = 0.5$, and $\lambda_o = \lambda_i = 0.2$.

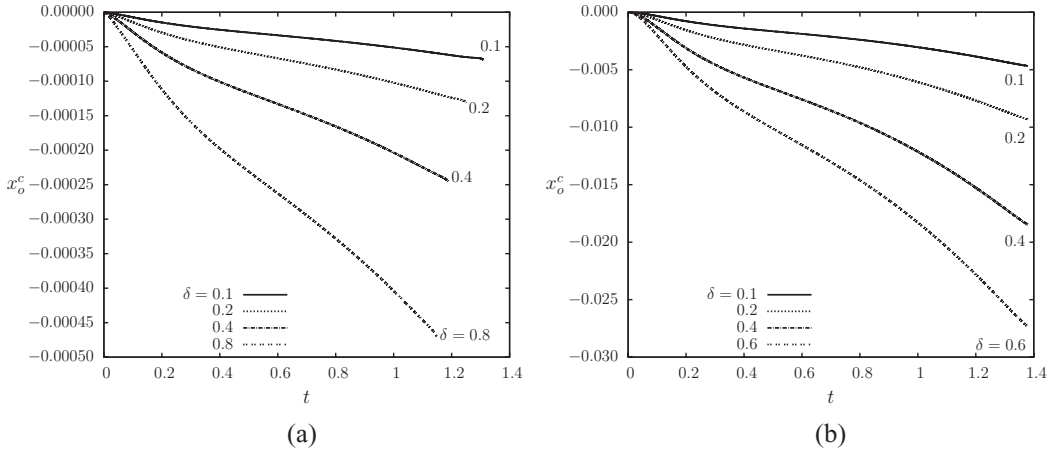

FIG. 22. Centroid location x_o^c of the outer droplet as a function of time t. The inner droplet is located on the x axis. The size ratios are (a) $k = 0.1$ and (b) $k = 0.39$. For all cases, $Ca_o = 0.1$, $\Gamma = 0.5$, and $\lambda_o = \lambda_i = 0.2$.

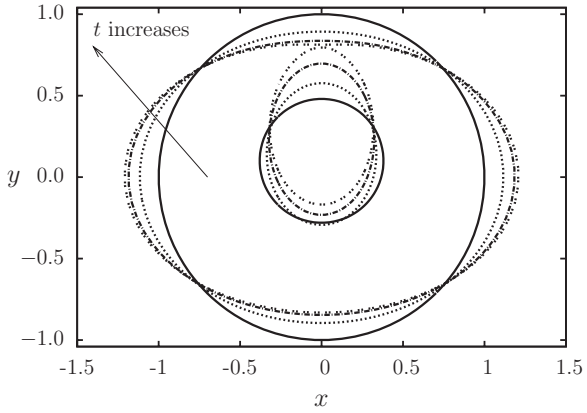

FIG. 23. Profiles of a compound droplet with the inner droplet initially located on y axis. Profiles presented are for time $t = 0, 0.1, 0.2, 0.25$. $Ca_o = 0.1$, $k = 0.38$, $\Gamma = 0.5$, $\lambda_o = \lambda_i = 0.2$, and $\delta = 0.1$.

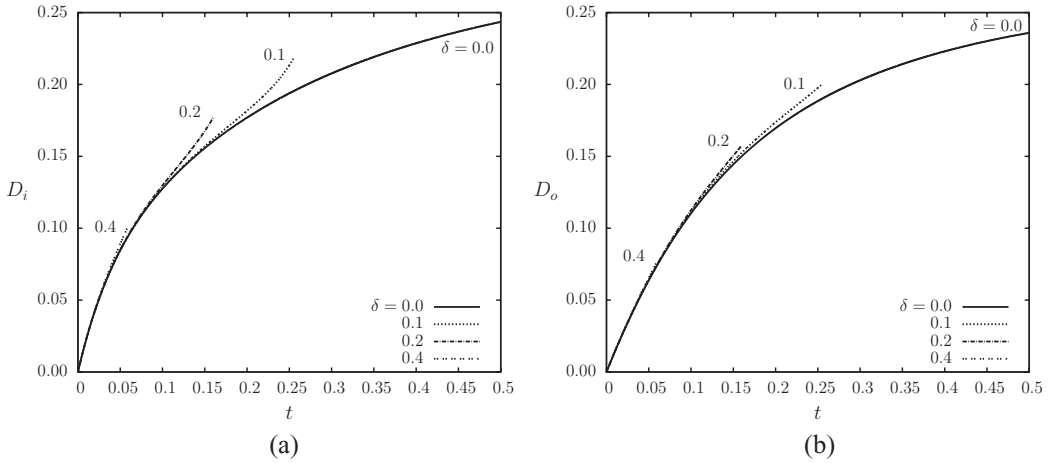

FIG. 24. Deformation (a) D_i and (b) D_o as a function of time t for a compound droplet with the inner droplet initially located on y axis. For all cases, $Ca_o = 0.1$, $k = 0.38$, $\Gamma = 0.5$, and $\lambda_o = \lambda_i = 0.2$.

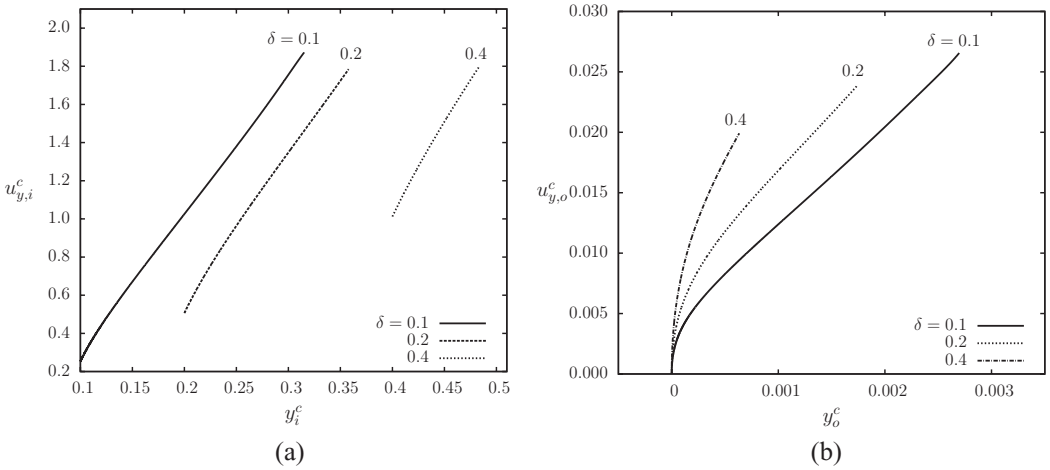

FIG. 25. Droplet centroid velocity (a) $u^c_{y,i}$ and (b) $u^c_{y,o}$ as a function of its location, y^c_i and y^c_o, respectively for a compound droplet with the inner droplet initially located on y axis. $Ca_o = 0.1$, $k = 0.38$, $\Gamma = 0.5$, and $\lambda_o = \lambda_i = 0.2$.

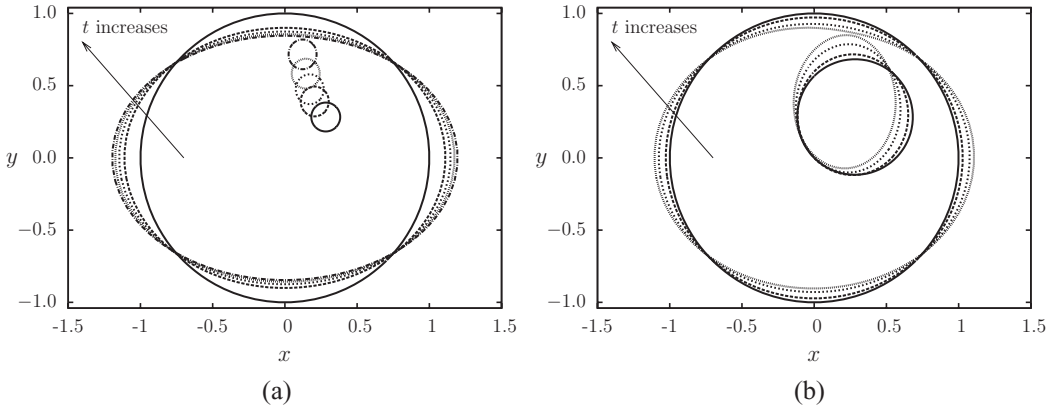

FIG. 26. Profiles of a compound droplet with the inner droplet centroid initially located on $y = x$ where $y > 0$ and $x > 0$. The size ratios are (a) $k = 0.1$ (b) $k = 0.4$. For all cases, $Ca_o = 0.1$, $\Gamma = 0.5$, $\lambda_o = \lambda_i = 0.2$ and $\delta = 0.4$.

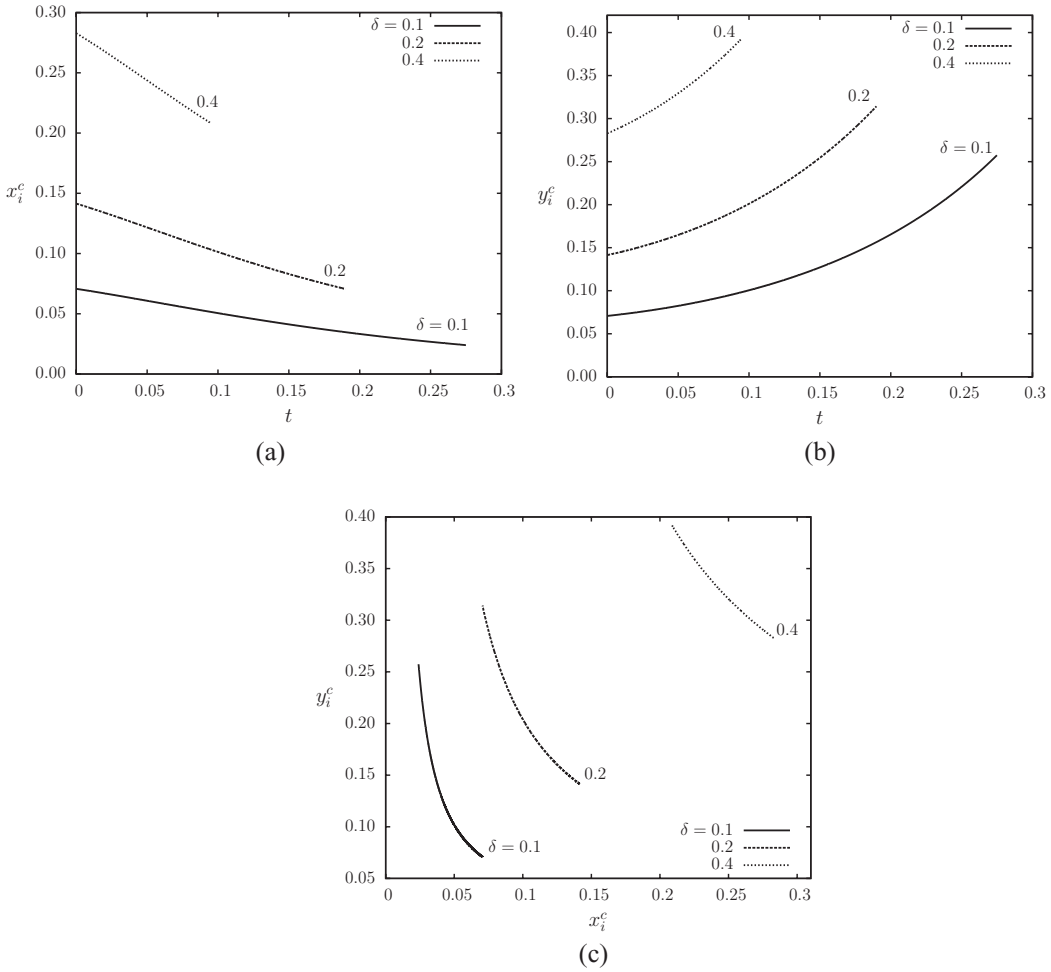

FIG. 27. Behavior of the inner droplet centroid for a compound droplet with the inner droplet centroid initially located on $y = x$ where $y > 0$ and $x > 0$. Coordinates of droplet centroid location x_i^c and y_i^c are plotted as a function of time t in (a) and (b), respectively. The trajectory of the inner droplet centroid is plotted in (c). Three cases are examined with the distance between the outer and inner droplets $\delta = 0.1, 0.2, 0.4$. For all cases, $Ca_o = 0.1$, $k = 0.4$, $\Gamma = 0.5$, and $\lambda_o = \lambda_i = 0.2$.

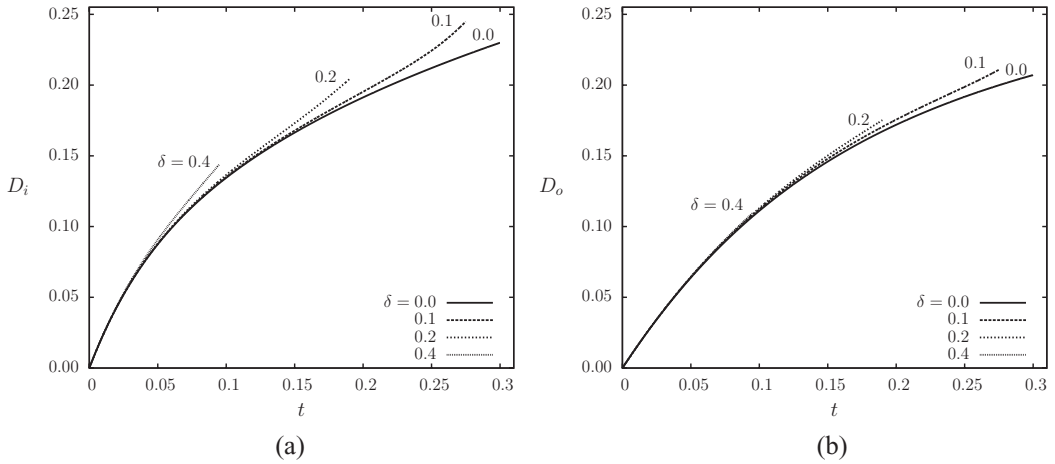

FIG. 28. Deformation (a) D_i and (b) D_o as a function of time t for a compound droplet with the inner droplet centroid initially located on $y = x$, where $y > 0$ and $x > 0$. For all cases, $Ca_o = 0.1$, $k = 0.4$, $\Gamma = 0.5$, $\lambda_o = \lambda_i = 0.2$.

for a compound droplet with the inner droplet centroid initially located at ($\delta \cos(\pi/4)$, $\delta \sin(\pi/4)$, 0). Since the inner droplet is offset in both x and y direction, the droplet moves towards the outer droplet centroid as it migrates to the outer interface. The y direction motion of the inner droplet leads to the contact of the two interfaces and prevents the existence of a completely engulfing compound droplet. We include in Fig. 26 profiles for both a small inner droplet ($k = 0.1$) and a larger inner droplet ($k = 0.4$). Similar behavior is observed for both cases although the latter exhibits a significant deformation for the inner droplet, which incurs an earlier contact between the two interfaces.

To quantify the inner droplet migration, we plot in Fig. 27 the droplet centroid location as a function of time as well as its trajectory. The centroid location of the inner droplet x_i^c decreases with time. The droplet with larger offset initially (i.e., larger value for δ) moves faster towards outer droplet centroid. Meanwhile, y_i^c increases with time and the droplet with a larger value for δ moves faster towards the outer interface. Figure 27(c) then shows the trajectory of the inner droplet centroid for three cases with different values of δ. The deformation of the inner and outer droplets is plotted in Fig. 28. The abrupt increase in the deformation D_i indicates the close contact of the two interfaces. The outer droplet deformation D_o also deviates from that of the concentric case (i.e., $\delta = 0$) due to the approach and contact of the inner interface.

IV. CONCLUSIONS

A three-dimensional spectral boundary element method has been employed to investigate the motion of a viscous compound droplet in a planar extensional flow. The numerical approach has been validated by comparing with analytical predictions and other numerical results. In addition, we compute the deformation of a compound droplet with a extremely small inner droplet and compare the deformation of the outer droplet with that of a correspondent simple droplet. The similar values in deformation of the two aforementioned cases again confirm the validity of the current algorithm.

In this study, the stability of a compound droplet in the planar extensional flow is investigated under the influences of inner droplet size, capillary number, relative surface tension of the inner droplet, as well as the initial location of the inner droplet. We find that given the same viscosities, surface tensions, and shear rate, both the inner and outer droplets deform more substantially if the inner droplet is larger. The increase in the size of the inner droplet leads to the instability of the compound droplet. The compound droplet with a smaller surface tension on the inner interface tends to deform more significantly for both the inner and outer droplet. A smaller inner surface tension also promotes the break-up of the entire compound droplet. We observe two break-up mechanism for compound droplets: (i) dimple development on the outer interface, pointing corner formed on the inner interface, and the resulting contact of the two interfaces; (ii) the extensive elongation of

the inner droplet, or the instability of the inner droplet alone. A large inner droplet with moderate deformation for the outer droplet may result in the first mechanism, while an inner surface tension which is less than the critical inner surface tension may incur the second mechanism. We also examine the influence of viscosity ratios on the steady-state droplet deformation by considering a wide range of values for the viscosities. The investigation reveals that the deformation of a stable compound droplet is affected by viscosity ratios only when the ratios are moderate. For moderate viscosity ratios, a compound droplet which has a more viscous "shell" exhibits larger deformation at steady state.

The influence of the initial location of the inner droplet on eccentric compound droplets is examined by computing with parameters which would give stable or unstable concentric droplets. Results show that the initial location of the inner droplet has negligible influence on the deformation of the outer droplet. However, the stability of the compound droplet may be affected by the initial location and/or the size of the inner droplet. For compound droplets suspended in a planar extensional flow as described in this study, no steady state could be found for completely engulfing droplets if the inner droplet has an initial offset in y direction. We also notice that the initially eccentrically located inner droplet results in not only the migration of the inner droplet but also the motion of the outer droplet. It is found that the outer droplet always moves in the same direction with the inner droplet although its velocity magnitude is in orders of magnitude smaller than that of the inner droplet. In addition, the compound droplet shows a faster migration speed if the inner droplet is located further away from the center of the outer droplet.

This study demonstrates the feasibility of the three-dimensional spectral boundary element method in the investigation of the dynamics of complex fluid, namely, compound droplets. The nature of this high-order numerical method facilitates the investigation for the dynamics of eccentric compound droplets in three dimensions, which is difficult to perform experimentally. Although streamlines in the fluid volume are not shown due to the fact that the numerical approach only solves for interfacial velocities, the flow velocity distributions in the fluid volume may be obtained independently based on current solutions, i.e., time dependent droplet configurations and interfacial velocities. In addition, this work provides foundation for future numerical studies on the dynamics of compound droplets, capsules, or blood cells in confined geometries.

ACKNOWLEDGMENTS

This work was supported by the Department of Energy under Award No. DE-FG52-08NA28921, National Science Foundation EPS-0814442 through ND EPSCoR, and the NDSU Development Foundation's Centennial Endowment award. Some computations were carried out on high performance computing systems at the Center for Computationally Assisted Science and Technology (CCAST) at North Dakota State University.

[1] M. L. Fabiilli, J. A. Lee, O. D. Kripfgans, P. L. Carson, and J. B. Fowlkes, "Delivery of water-soluble drugs using acoustically triggered perfluorocarbon double emulsions," Pharm. Res. **27**, 2753–2765 (2010).
[2] Y. H. Lee, C. A. Kim, W. H. Jang, H. J. Choi, and M. S. Jhon, "Synthesis and electrorheological characteristics of microencapsulated polyaniline particles with melamine-formaldehyde resins," Polymer **42**, 8277–8283 (2001).
[3] N. N. Li, "Permeation through liquid surfactant membranes," AIChE J. **17**, 459–463 (1971).
[4] L. Sapei, M. A. Naqvi, and D. Rousseau, "Stability and release properties of double emulsions for food applications," Food Hydrocolloids **27**, 316–323 (2012).
[5] T. V. Vasudevan and M. S. Naser, "Some aspects of stability of multiple emulsions in personal cleaning systems," J. Colloid Interface Sci. **256**, 208–215 (2002).
[6] S. Tasoglu, G. Kaynak, A. J. Szeri, U. Demirci, and M. Muradoglu, "Impact of a compound droplet on a flat surface: A model for single cell epitaxy," Phys. Fluids **22**, 082103 (2010).
[7] S. Moon, S. K. Hasan, Y. S. Song, F. Xu, H. O. Keles, F. Manzur, S. Mikkilineni, J. W. Hong, J. Nagatomi, E. Haeggstrom, A. Khademhosseini, and U. Demirci, "Layer by layer three-dimensional tissue epitaxy by cell-laden hydrogel droplets," Tissue Eng. Part C Methods **16**, 157–166 (2010).
[8] H. C. Kan, H. S. Udaykumar, W. Shyy, and R. Tran-Son-Tay, "Hydrodynamics of a compound drop with application to leukocyte modeling," Phys. Fluids **10**, 760–774 (1998).
[9] H. C. Kan, W. Shyy, H. S. Udaykumar, P. Vigneron, and R. Tran-Son-Tay, "Effects of nucleus on leukocyte recovery," Ann. Biomed. Eng. **27**, 648–655 (1999).

[10] H. C. Kan, H. S. Udaykumar, W. Shyy, and R. Tran-Son-Tay, "Numerical analysis of the deformation of an adherent drop under shear flow," J. Biomech. Eng. **121**, 160–169 (1999).
[11] D. B. Khismatullin and G. A. Truskey, "Three-dimensional numerical simulation of receptor-mediated leukocyte adhesion to surfaces: Effects of cell deformability and viscoelasticity," Phys. Fluids **17**, 032505 (2005).
[12] V. Pappu and P. Bagchi, "3D computational modeling and simulation of leukocyte rolling adhesion and deformation," Comput. Biol. Med. **38**, 738–753 (2008).
[13] K. A. Smith, F. J. Solis, L. Tao, K. Thornton, and M. O. de la Cruz, "Domain growth in ternary fluids: A level set approach," Phys. Rev. Lett. **84**, 91–94 (2000).
[14] H. Chen, J. Li, H. C. Shum, H. A. Stone, and D. A. Weitz, "Breakup of double emulsions in constrictions," Soft Matter **7**, 2345–2347 (2011).
[15] S. Torza and S. G. Mason, "Three-phase interactions in shear and electrical fields," J. Colloid Interface Sci. **33**, 67–83 (1970).
[16] R. E. Johnson and S. S. Sadhal, "Fluid mechanics of compound multiphase drops and bubbles," Annu. Rev. Fluid Mech. **17**, 289–320 (1985).
[17] A. M. J. Davis and H. Brenner, "Emulsions containing a third solid internal phase," J. Engrg. Mech. Div. **107**, 609–621 (1981).
[18] S. S. Sadhal and R. E. Johnson, "Stokes flow past bubbles and drops partially coated with thin films. Part 1. Stagnant cap of surfactant film - exact solution," J. Fluid Mech. **126**, 237–250 (1983).
[19] E. Rushton and G. A. Davies, "Settling of encapsulated droplets at low Reynolds numbers," Int. J. Multiphase Flow **9**, 337–342 (1983).
[20] S. S. Sadhal and H. N. Oguz, "Stokes flow past compound multiphase drops: the case of completely engulfed drops/bubbles," J. Fluid Mech. **160**, 511–529 (1985).
[21] H. A. Stone and L. G. Leal, "Breakup of concentric double emulsion droplets in linear flows," J. Fluid Mech. **211**, 123–156 (1990).
[22] K. A. Smith, J. M. Ottino, and M. O. de la Cruz, "Encapsulated drop breakup in shear flow," Phys. Rev. Lett. **93**, 204501 (2004).
[23] C. Pozrikidis, *Boundary Integral and Singularity Methods for Linearized Viscous Flow* (Cambridge University Press, New York, 1992).
[24] Y. Wang and P. Dimitrakopoulos, "A three-dimensional spectral boundary element algorithm for interfacial dynamics in Stokes flow," Phys. Fluids **18**, 082106 (2006).
[25] M. A. Khan and Y. Wang, "Droplet motion in a microconfined shear flow via a three-dimensional spectral boundary element method," Phys. Fluids **22**, 123301 (2010).
[26] Y. Wang and P. Dimitrakopoulos, "Low-Reynolds-number droplet motion in a square microfluidic channel," Theor. Comput. Fluid Dyn. **26**, 361–379 (2012).